

**Influence of projectile breakup on the  $^{16}\text{O} + ^{115}\text{In}$  reaction at energies  $\approx 4\text{--}7$  MeV/nucleon**Kamal Kumar,<sup>1,\*</sup> Tauseef Ahmad,<sup>1</sup> Sabir Ali,<sup>1</sup> I. A. Rizvi,<sup>1,†</sup> Avinash Agarwal,<sup>2</sup> R. Kumar,<sup>3</sup> and A. K. Chaubey<sup>4</sup><sup>1</sup>*Department of Physics, Aligarh Muslim University, Aligarh, Uttar Pradesh 202 002, India*<sup>2</sup>*Department of Physics, Bareilly College, Bareilly, Uttar Pradesh 243 005, India*<sup>3</sup>*NP Group, Interuniversity Accelerator Centre, New Delhi, India*<sup>4</sup>*Department of Physics, Addis Ababa University, Post Office Box 1176, Addis Ababa, Ethiopia*

(Received 25 July 2013; revised manuscript received 13 November 2013; published 26 December 2013)

To study the influence of breakup on fusion of  $^{16}\text{O}$  projectile with  $^{115}\text{In}$  target, a well-established activation technique has been employed to measure the excitation functions at low incident energies. The analysis of the present study has been carried out in the framework of the statistical model code PACE4. The corrected yields after precursor contribution subtraction for all the measured  $pxn$  channels were consistent with the theoretical predictions and attributed to the complete fusion processes. However, a significant enhancement in the measured excitation functions of  $\alpha$ -emitting channels was observed and assigned to the incomplete fusion of the projectile. The estimated incomplete fusion fraction has been used to study the effect of several entrance channel parameters on incomplete fusion reaction dynamics.

DOI: [10.1103/PhysRevC.88.064613](https://doi.org/10.1103/PhysRevC.88.064613)

PACS number(s): 25.70.Jj, 25.70.Gh, 25.70.Mn

**I. INTRODUCTION**

During the past decade, the role of incomplete fusion (ICF) in light- and heavy-ion-induced reactions at low projectile energies has been a subject of current interest, particularly at energies near the Coulomb barrier (CB), where ICF was found to compete with complete fusion (CF) [1–6]. Interest in the investigation of the effect of breakup on fusion has also increased in recent years, as the existence of ICF [7–10] and fission and quasifission [11–14] at low incident energies adds complexity to the synthesis of superheavy elements.

In a qualitative way, CF and ICF processes can be disentangled on the basis of driving input angular momenta [15–17]. In a sharp cutoff approximation, the probability of CF is assumed to be unity for  $l \leq l_{\text{crit}}$  and expected to be zero for  $l > l_{\text{crit}}$  [15,16]. However, at relatively higher projectile energies and at the finite values of the impact parameters, CF gradually gives way to ICF, where fractional mass and charge as well as the linear momentum of projectile are transferred to the target nucleus, due to the prompt emission of  $\alpha$  clusters in the forward cone with almost projectile velocity. However, recently Yadav *et al.* [18] has observed the existence of ICF reaction dynamics at  $l < l_{\text{crit}}$ , which suggests a diffused boundary that may penetrate near the barrier. The ICF reaction processes were first observed by Britt and Quinton [19] in the bombardment of heavy targets by  $^{12}\text{C}$ ,  $^{14}\text{N}$ , and  $^{16}\text{O}$  projectiles at energies well above the CB. Later on, particle- $\gamma$  coincidence studies by Inamura *et al.* [20] contributed a great deal to our understanding of the underlying reaction dynamics. They measured charged particle- $\gamma$  coincidences and found that at least a fraction of the fast  $\alpha$  particles observed in the  $^{14}\text{N} + ^{159}\text{Tb}$  reaction at 95 MeV may be produced in ICF reactions. This happens when a massive fragment of the projectile (e.g.,  $^{10}\text{B}$ ) is captured by the target nucleus and only its remaining part (e.g., an  $\alpha$  particle) continues to move in the forward direction.

To explain the mechanism of ICF reaction dynamics, a number of theoretical models [21–24] have been proposed. In reality, these proposed models qualitatively explain the experimental data at energies  $\approx 10$  MeV/nucleon and hence a reasonable justification is still needed to reproduce the experimental data obtained at energies as low as  $\approx 4\text{--}7$  MeV/nucleon. Further, Parker *et al.* [25] observed forward-peaked  $\alpha$  particles in low- $Z$  heavy-ion interactions on a  $^{51}\text{V}$  target at energies  $\approx 6$  MeV/nucleon.

Recently, several studies have drawn the attention to the dependence of ICF reaction dynamics on various entrance channel parameters. The observations in Refs. [26,27] show that the probability of projectile breakup increases with the increasing input-driven angular momentum and projectile energy. Some recent studies proposed ICF reaction dynamics as a function of  $Z_P Z_T$  of the interacting partners [7] and the target charge  $Z_T$  [28]. Morgenstern *et al.* [29] correlated the ICF fraction with entrance channel mass asymmetry. In addition to this, most of the recent studies [30–32] report that  $\alpha$ - $Q$  value of the projectile is also responsible for the projectile breakup.

The  $^{12}\text{C}$ ,  $^{16}\text{O}$ , and  $^{20}\text{Ne}$  projectiles, which are considered to have  $\alpha$ -cluster structures, have been used in most of the previous studies. In fact the cluster structure has been suggested as one of the factors leading to forward-peaked  $\alpha$  particles in ICF reactions. Moreover, recently we have observed [31,32] that projectiles having bigger  $\alpha$ -cluster structures have greater ICF probability. This aspect needs more experimental verification in different target mass regions. In view of the above, we have measured the excitation functions (EFs) for the evaporation residues in  $^{16}\text{O} + ^{115}\text{In}$  system with projectile energies from just above the CB to well beyond it. The target ( $^{115}\text{In}$ ) was chosen because many of the possible evaporation residues produced in the reaction of  $^{16}\text{O}$  with this target have half-lives and decay properties suitable for the off-line measurements. This study also give strength to the concept of projectile structure dependence of ICF reaction dynamics in medium-mass target region. Therefore, the objective of this work is to understand the ambiguous dependency of ICF

\*kamalkumar1908@gmail.com

†isarrizvi@hotmail.com

reaction dynamics on different entrance channel parameters. In this regard, to draw more conclusions about ICF reactions, we have reanalyzed nearby target-projectile systems [28,33–37] in light of the present work. The present work reflects the impact of various entrance channel parameters on ICF reaction dynamics in the vicinity of the Coulomb barrier.

## II. EXPERIMENTAL DETAILS

The experiment was carried out using the pelletron facility at the Inter University Accelerator Center (IUAC), New Delhi, India. A stack of six self-supporting targets consisting of two isotopes of natural indium,  $^{115}\text{In}$  (95.7%)+ $^{113}\text{In}$  (4.3%), was prepared. The target was spectroscopically 99.99% pure. Each target was  $\approx 1\text{ mg/cm}^2$  thick backed with Al foils  $\approx 1.8\text{--}2.1\text{ mg/cm}^2$  thick and was prepared using the rolling technique. These Al foils trap the recoiling products and the energy degrader to cover the desired energy range. The thickness of each target and catcher foil was separately measured through weighing and by an  $\alpha$ -transmission method, respectively. The incident beam energy on each target foil in the stack has been estimated using the SRIM code [38]. Due to very low abundance of  $^{113}\text{In}$ , we have rejected the contribution on account of this isotope, which is considerable only at low incident energies.

To measure the EFs of various evaporation residues produced in the  $^{16}\text{O}+^{115}\text{In}$  system, the stack has been irradiated for  $\approx 8\text{ h}$  in the General Purpose Scattering Chamber (GPSC) using the in-vacuum transfer facility, keeping in mind the half-lives of interest. An average beam current  $\approx 30\text{--}35\text{ nA}$  was maintained throughout the experiment. The current was monitored by a Faraday cup installed behind the stack. A precalibrated HPGe detector coupled to a CAMAC-based FREEDOM data acquisition system developed by the IUAC [39] has been used to measure the induced activity in the target-catcher assembly. The nuclear spectroscopic data used in the evaluation and measurements of cross sections have been taken from the Radioactive Isotopes Data Table of Brown and Firestone [40] and are given in Table I. A typical  $\gamma$ -ray spectrum for the  $^{16}\text{O}+^{115}\text{In}$  system at  $\approx 96.4\text{ MeV}$  is presented in Fig. 1, where several  $\gamma$  peaks corresponding to different reaction products via CF and/or ICF channels are indicated. These residues are identified on the basis of decay curve analysis, and a typical representation is shown in the inset of Fig. 1. The geometry-dependent efficiency of the detector has been determined using a  $^{152}\text{Eu}$  source at various source-detector separations. The various factors that may introduce errors and uncertainties in the present cross-sectional measurements and their estimates are the following: (i) The nonuniformity in the thickness of the samples may cause uncertainty in determination of the number of target nuclei. The estimated error in the thickness of the sample materials is less than 1%. (ii) Fluctuation in the beam current may lead to variation of the incident flux. Hence, proper care was taken to keep the beam current constant as much as possible. The weighted average of the beam current has been taken to estimate the error due to this factor, which is found to be less than 2%. (iii) Due to the dead time in the spectrometer, counts may be lost. By suitably adjusting the sample-detector distance, the dead time was kept below 10%. (iv) Uncertainty in

TABLE I. List of reactions with their residues and spectroscopic properties.

Residue	$T_{1/2}$	$J^\pi$	$E_\gamma$ (keV)	$I^\gamma$
$^{129}\text{Ba}^g(pn)$	2.23 h	$1/2^+$	214.3 129.1	13.4 5.51
$^{129}\text{Ba}^m(pn)$	2.16 h	$7/2^+$	182.3	100.0 <sup>a</sup>
$^{128}\text{Ba}(p2n)$	2.43 d	$0^+$	273.4	15.0
$^{127}\text{Ba}(p3n)$	12.7 min	$1/2^+$	180.8 114.8	12.0 9.3
$^{126}\text{Ba}(p4n)$	100.0 min	$0^+$	233.6	19.6
$^{127}\text{Cs}(\alpha)$	6.25 h	$1/2^+$	411.8	63.0
$^{125}\text{Cs}(\alpha 2n)$	45.0 min	$1/2^+$	526.0 111.8	24.0 9.0
$^{125}\text{Xe}(\alpha pn)$	16.9 h	$1/2^+$	188.4	54.0
$^{123}\text{Xe}(\alpha p 3n)$	2.08 h	$1/2^+$	148.9 178.1	49.0 14.9
$^{122}\text{Xe}(\alpha p 4n)$	20.1 h	$0^+$	350.0	7.8
$^{121}\text{Xe}(\alpha p 5n)$	40.1 min	$5/2^+$	252.7 445.2	13.0 7.7
$^{121}\text{I}(2\alpha 2n)$	2.12 h	$5/2^+$	212.2	84.0
$^{120}\text{I}^s(2\alpha 3n)$	81.0 min	$2^-$	560.4 601.1	73.0 5.8
$^{120}\text{I}^m(2\alpha 3n)$	53.0 min	4 to 8	560.4 601.1	100.0 <sup>a</sup> 87.0 <sup>a</sup>
$^{119}\text{I}(2\alpha 4n)$	19.1 min	$5/2^+$	257.5	87.0 <sup>a</sup>
$^{118}\text{Sb}^m(3\alpha n)$	5.00 h	$8^-$	1050.0 1229.0	97.0 <sup>a</sup> 100.0 <sup>a</sup>
$^{117}\text{Sb}(3\alpha 2n)$	2.80 h	$5/2^+$	158.5	86.0 <sup>a</sup>
$^{116}\text{Sb}^m(3\alpha 3n)$	60.3 min	$8^-$	1293.5 972.6	100.0 <sup>a</sup> 74.2 <sup>a</sup>

<sup>a</sup>These intensities are relative.

determining the geometry-dependent detector efficiency may also cause some error, which is estimated to be less than 2%. (v) Errors due to a decrease in the oxygen ion beam intensity caused by scattering while transferring through the stack are estimated to be less than 1%. These errors exclude uncertainty of the nuclear data, such as branching ratio and decay constant, which have been taken from Ref. [40]. Attempts were made

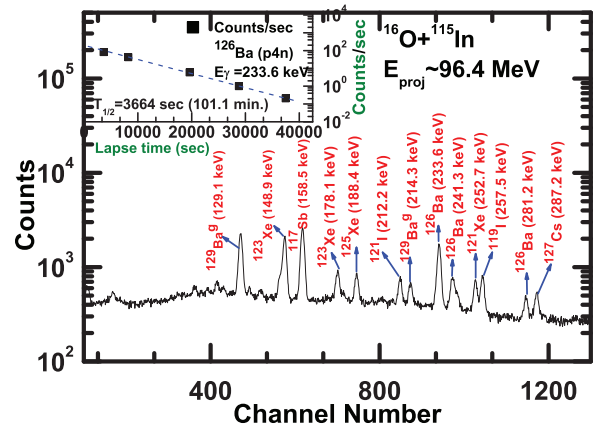


FIG. 1. (Color online) Typical spectrum of  $^{16}\text{O}+^{115}\text{In}$  system using projectile beam of  $\approx 96.4\text{ MeV}$  energy. In the inset, a typical curve identifies  $^{126}\text{Ba}$  residue through its half-life.

to minimize the uncertainties caused by the above factors. The overall errors in the present work have been estimated to be less than or equal to 17%.

### III. RESULTS AND DISCUSSION

The interaction of  $^{16}\text{O}$  projectile with  $^{115}\text{In}$  results in a compound nucleus,  $^{131}\text{La}^*$ , which further de-excites into different evaporation residues. A few recent studies have observed that for tightly bound projectiles, such as  $^{16}\text{O}$ ,  $\sigma_R$  (total reaction cross section) is approximately equal to  $\sigma_{\text{TF}}$  (total fusion cross section) [7,41,42]. Generally,  $\sigma_R$  also includes  $\sigma_{\text{EBU}}$  (elastic breakup cross section) along with  $\sigma_{\text{TF}}$  for weakly bound projectiles. This value of  $\sigma_{\text{EBU}}$  is found negligible in the case of tightly bound projectiles [7,41,42]. Most of the experiments give the total fusion (TF) cross section, corresponding to the sum of complete fusion ( $\sigma_{\text{CF}}$ ) and incomplete fusion ( $\sigma_{\text{ICF}}$ ) cross sections [2,3,26,27,31]. However, the statistical model code PACE4 [43] calculates  $\sigma_{\text{CF}}$  only, and therefore we have done further analysis using the same code. The enhanced cross section may be assigned to the ICF contribution.

In order to study the influence of projectile breakup on ICF reaction dynamics at low incident energies in  $^{16}\text{O}+^{115}\text{In}$  system, the EFs for  $^{129g,129m,128-126}\text{Ba}$ ,  $^{127,125}\text{Cs}$ ,  $^{125,123-121}\text{Xe}$ ,  $^{121,120g,120m,119}\text{I}$ , and  $^{118m,117,116m}\text{Sb}$  residues, populated via CF and/or ICF, have been measured. The standard formulation reported in Ref. [5] has been used to determine the production cross sections of various reaction products. A residue may be populated via a specific channel often emitting several  $\gamma$  rays of different energies. Hence, the reported values of the cross sections for some residues are the weighted average [44] of cross sections obtained for their different  $\gamma$  rays.

#### A. Analysis with statistical model code PACE4

The experimentally obtained EFs for  $^{129g,129m,128-126}\text{Ba}$  evaporation residues expected to be populated via emission of  $pxn$  ( $x = 1-4$ ) from the excited composite nucleus  $^{131}\text{La}^*$  in the interaction of  $^{16}\text{O}$  with  $^{115}\text{In}$  are shown in Fig. 2(a). These evaporated residues are identified on the basis of their half-lives and characteristic  $\gamma$ -ray energies. All these  $pxn$  channels are expected to be populated both ways, namely, decay through their higher charge isobar precursors at their diagonal positions in the periodic table via  $\beta^+$  decay and/or electron capture (EC). In the present case, the half-lives of the precursors are considerably smaller than those of the residues. Hence, the independent cross sections of these residues have been determined by analyzing the induced activities of their precursors using the decay analysis introduced by Cavinato *et al.* [45].

If a precursor  $P$  is formed with cross section  $\sigma_P$  during the irradiation and decays with half-life  $t_{1/2}^P$  and a branching ratio  $P_{\text{pre}}$  to a daughter nucleus  $D$  which is produced with half-life  $t_{1/2}^D$ , the cumulative cross section  $\sigma_{\text{cum}}$  in terms of independent yield  $\sigma_{\text{ind}}$  for the production of a daughter is given by

$$\sigma_{\text{cum}} = \sigma_{\text{ind}} + P_{\text{pre}} \left[ \frac{t_{1/2}^D}{t_{1/2}^D - t_{1/2}^P} \right] \sigma_P. \quad (1)$$

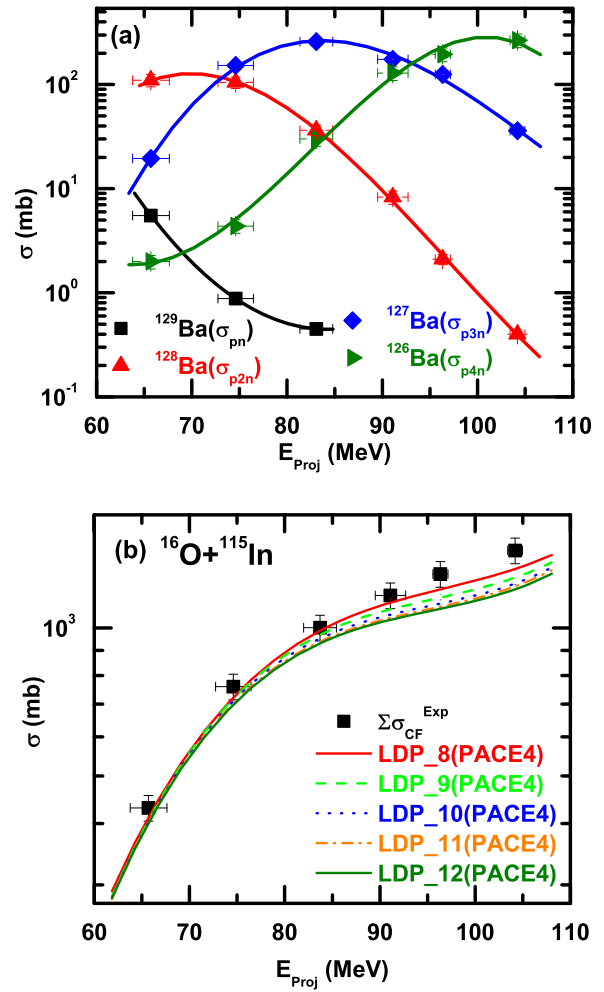


FIG. 2. (Color online) (a) Measured EFs for all  $pxn$  ( $x = 1-4$ ) channels. In this figure various solid lines join the experimental data points to guide the eyes. (b) Sum of all CF channels along with PACE4 calculations (for  $K = 8-12$ ).

The measured yield of  $p2n$  channel is cumulative. So, by using the above formulation, the independent yield of  $^{128}\text{Ba}$  can be calculated as follows:

$$\sigma_{\text{cum}}(^{128}\text{Ba}) = \sigma_{\text{ind}}(^{128}\text{Ba}) + 1.001\sigma_P(^{128}\text{La}). \quad (2)$$

Similarly, the independent yields of two other  $pxn$  channels, i.e.,  $^{127}\text{Ba}$  and  $^{126}\text{Ba}$ , may also be deduced as

$$\sigma_{\text{cum}}(^{127}\text{Ba}) = \sigma_{\text{ind}}(^{127}\text{Ba}) + 1.671\sigma_P(^{127}\text{La}) \quad (3)$$

and

$$\sigma_{\text{cum}}(^{126}\text{Ba}) = \sigma_{\text{ind}}(^{126}\text{Ba}) + 1.009\sigma_P(^{126}\text{La}). \quad (4)$$

Here,  $P_{\text{pre}} = 1$  [40]. The experimentally measured independent yields of all  $pxn$  channels have also been tabulated in Table II.

In order to justify the experimental measurement of EFs via  $pxn$  channels, the present analysis has been carried out in the framework of the statistical model code PACE4 [43]. This code is based on Hauser-Feshbach formalism [46]. The evaporation cross sections are calculated by using the Bass formula [47]. The optical model potentials of Becchetti

TABLE II. Experimentally measured production reaction cross sections  $\sigma$  (mb) for all CF as well as  $\alpha$ -emitting channels.

$E_{\text{lab}}$ (MeV)	$^{129}\text{Ba}^{\alpha+m}$ (mb)	$^{128}\text{Ba}$ (mb)	$^{127}\text{Ba}$ (mb)	$^{126}\text{Ba}$ (mb)	$^{127}\text{Cs}$ (mb)	$^{125}\text{Cs}$ (mb)	$^{125}\text{Xe}$ (mb)	$^{123}\text{Xe}$ (mb)	$^{122}\text{Xe}$ (mb)
$65.7 \pm 1.93$	$5.6 \pm 0.7$	$110.0 \pm 15.0$	$19.6 \pm 1.75$	$1.99 \pm 0.3$	$7.1 \pm 1.1$	$8.7 \pm 1.3$	$3.7 \pm 0.44$		$5.8 \pm 0.9$
$74.6 \pm 1.87$	$0.9 \pm 0.1$	$105.0 \pm 13.0$	$152.6 \pm 13.7$	$4.4 \pm 0.7$	$60.7 \pm 9.1$	$14.2 \pm 2.1$	$5.3 \pm 0.63$	$7.8 \pm 1.2$	$3.6 \pm 0.5$
$83.2 \pm 1.72$	$0.5 \pm 0.06$	$36.5 \pm 1.7$	$258.5 \pm 23.2$	$30.1 \pm 4.5$	$55.5 \pm 8.3$	$16.5 \pm 2.5$	$7.0 \pm 0.75$	$14.8 \pm 2.2$	$4.9 \pm 0.7$
$91.1 \pm 1.60$		$8.3 \pm 1.2$	$175.03 \pm 15.7$	$128.8 \pm 19.3$	$73.9 \pm 11.1$	$25.2 \pm 3.8$	$8.6 \pm 1.0$	$76.5 \pm 11.5$	$7.5 \pm 1.1$
$96.3 \pm 0.80$		$2.1 \pm 0.3$	$125.2 \pm 10.6$	$195.0 \pm 29.2$	$33.3 \pm 4.9$	$35.8 \pm 5.37$	$13.3 \pm 1.6$	$114.3 \pm 17.2$	$15.8 \pm 1.6$
$105.0 \pm 0.78$		$0.4 \pm 0.03$	$36.0 \pm 2.7$	$266.5 \pm 39.9$	$15.7 \pm 2.4$	$115.0 \pm 17.2$	$25.0 \pm 3.0$	$150.0 \pm 22.5$	$59.5 \pm 8.9$

and Greenlees [48] are used for calculating the transmission coefficients for neutrons and protons, and the optical model potential of Satchler [49] is used for  $\alpha$ -particle emissions. In the description of  $\gamma$ -ray competitions, emissions of  $E_1$ ,  $E_2$ ,  $M_1$ , and  $M_2$   $\gamma$  rays are included and strengths for these transitions are taken from the tables of Endt [50]. The  $\gamma$ -decay intensities in Weisskopf units are  $E_1 = 0.000046$ ,  $M_1 = 0.007000$ ,  $E_2 = 7.700000$ , and  $M_2 = 0.058000$  for the  $^{16}\text{O}+^{115}\text{In}$  system. The ground-state deformation is taken as  $4\hbar$ , and the value of the fission barrier is taken as 42.18 MeV throughout the calculations.

Figure 2(b) shows a comparison of the total experimentally measured cross section of all  $pxn$  channels (i.e.,  $\Sigma\sigma_{\text{CF}}^{\text{expt.}}$ ) with PACE4 predictions (i.e.,  $\Sigma\sigma_{\text{CF}}^{\text{theo.}}$ ). In this code, the level density parameter ( $a = A/K$ ), is one of the important parameters, where  $A$  is the atomic mass number of the compound nucleus (CN) and  $K$  is a free parameter. The prescription of Kataria *et al.* [51] for the level density is employed for this purpose, which takes into account the excitation energy dependence of the level density parameter ( $a$ ), which suggests a level density parameter  $a = A/8 \text{ MeV}^{-1}$  for the studied energy region. Also, a value of level density parameter ( $a = A/8 \text{ MeV}^{-1}$ ) has also been suggested by Cavinato *et al.* [45] for nuclei far from the magic region. In some recent studies [3,5] with targets of lower mass,  $K = 10$  value is found most suitable as suggested by Fabris *et al.* [52]. Hence, we tested the values of level density parameter from  $A/8$  to  $A/12 \text{ MeV}^{-1}$ , to fit the experimental data, and the value  $A/8 \text{ MeV}^{-1}$  is most suitable for the present work, as indicated in Fig. 2(b). Hence, further analysis has been carried out with this value. The most important input parameters used to perform the PACE4 calculations are listed in Table III. In the case of  $\alpha$ -emitting channels the enhancement over the theoretical predictions may be attributed to the ICF processes, as suggested by several recent studies [1,2,10,13]. Therefore, the following attempt has been made.

TABLE III. The important input parameters used to perform the PACE4 calculations.

$E_{\text{lab}}$ (MeV)	Bass fusion cross section (mb)	Fusion radius (fm)	Yrast spin ( $\hbar$ )	$\ell_{\text{max}}$ ( $\hbar$ )
$65.70 \pm 1.93$	407	10.10	68	21
$72.90 \pm 1.87$	733	9.85	73	31
$83.20 \pm 1.72$	966	9.65	78	38
$91.90 \pm 1.60$	1144	9.40	83	43
$96.35 \pm 0.80$	1218	9.25	85	46
$105.00 \pm 0.78$	1316	7.75	89	50

To support our measurements and the adopted data reduction procedure, an attempt has been made to deduce the value of fusion barrier ( $V_{\text{CB}}$ ) (in the center-of-mass system) from the analysis of experimentally measured complete fusion cross section. According to Gutbrod *et al.* [53], the normalized CF probability may be given as

$$\Sigma\sigma_{\text{CF}} = \pi R_{\text{int}}^2 (1 - V_{\text{CB}}/E_{c.m.}) \quad (5)$$

The normalized values of  $\Sigma\sigma_{\text{CF}}$  is plotted as a function of  $1/E_{c.m.}$  in Fig. 3. As shown in this figure, the data points follow a straight-line trajectory which intersects the  $x$  axis at  $E_{c.m.}$  (projectile energy in the center-of-mass system) corresponding to 49.4 MeV. This corresponds to the value of fusion barrier ( $V_{\text{CB}} \approx 50.5 \text{ MeV}$ ) of the  $^{16}\text{O}+^{115}\text{In}$  system and strengthens the present measurements and the data reduction procedure.

## B. Projectile breakup processes and ICF contribution

### 1. $\alpha$ -emitting channels

The experimentally measured EFs for  $\alpha$ -emitting channels such as  $^{127,125}\text{Cs}$  are shown in Figs. 4(a) and 4(b). Due to the involvement of  $\alpha$ -particle emission, both CF and ICF are considered to be responsible for reaction modes, namely, (i) by CF of  $^{16}\text{O}$  followed by the formation of an excited compound nucleus  $^{131}\text{La}^*$ , from which evaporation of neutrons, protons, and  $\alpha$  particles may take place, or (ii) first  $^{16}\text{O}$  breaks into  $\alpha$

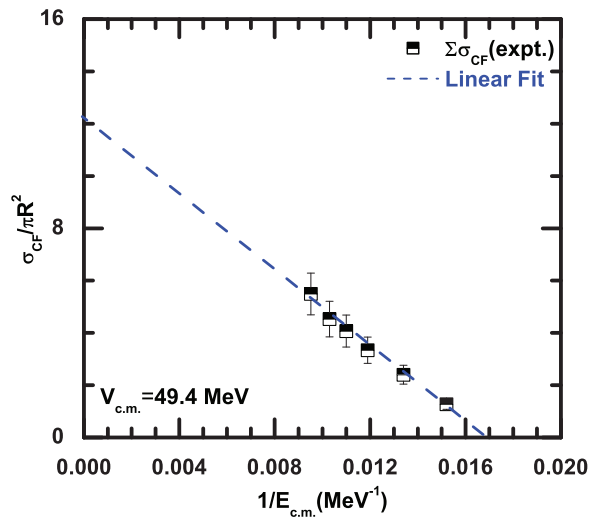


FIG. 3. (Color online) CF cross sections as the function of  $1/E_{c.m.}$  found to reproduce the Coulomb barrier for  $^{16}\text{O}+^{115}\text{In}$  system. The dashed line through the data points is achieved by best fitting procedure of data.

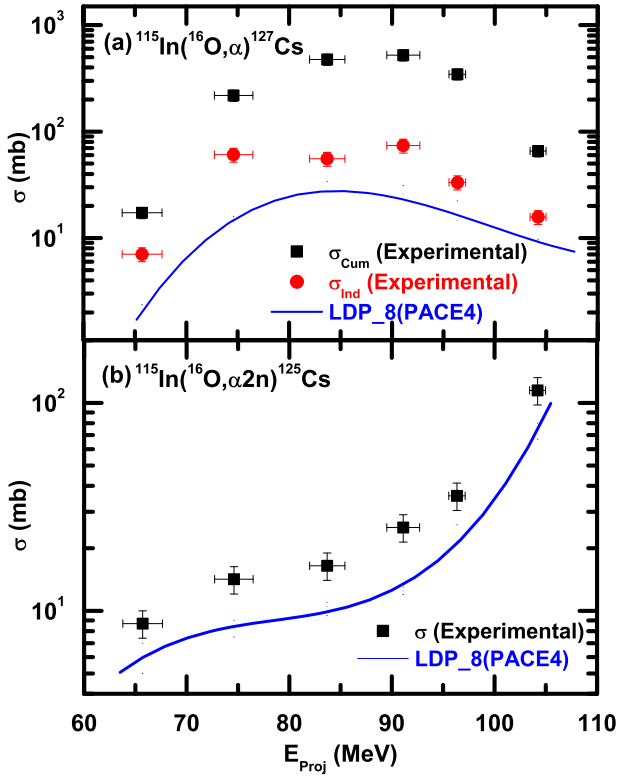
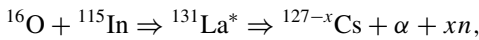


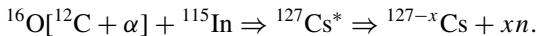
FIG. 4. (Color online) Experimentally measured EFs of  $^{127}\text{Cs}$  ( $\alpha$ ) and  $^{125}\text{Cs}$  ( $\alpha 2n$ ) are shown and compared with the theoretical predictions of code PACE4. The cumulative yield of  $^{127}\text{Cs}$  residue is also depicted.

clusters in the nuclear field of  $^{115}\text{In}$  target such as ( $\alpha + ^{12}\text{C}$ ) or ( $^8\text{Be} + ^8\text{Be}$ ) and then one of the fragments fuses with the target and the other fragment goes into the forward direction elastically. In this case the excited composite system is less in mass and charge than that in case of CF and hence is here referred to as ICF. Therefore, the reaction mechanism for the population of all observed  $\alpha$ -emitting channels in this case is expected to be CF and/or ICF and can be represented as

(i) CF of  $^{16}\text{O}$ , i.e.,



(ii) ICF of  $^{12}\text{C}$ , i.e.,



( $\alpha$  as spectator).

The EFs for  $^{127}\text{Cs}$  and  $^{125}\text{Cs}$  are plotted in Figs. 4(a) and 4(b). Moreover, the half-life of residue  $^{127}\text{Cs}$  is larger than that of its immediate precursor (i.e.,  $^{127}\text{Ba}$  isotope), so this isotope may be produced both ways independently, as well as through decay of its higher charge isobar precursors. The cumulative cross sections of this residue are also shown in Fig. 4(a). Therefore, in order to evaluate independent yield of  $^{127}\text{Cs}$  isotope, the same procedure has been used as in the previous section [45] and can be evaluated by using the following equation:

$$\sigma_{\text{cum}}(^{127}\text{Cs}) = \sigma_{\text{ind}}(^{127}\text{Cs}) + 1.035\sigma_P(^{127}\text{Ba}). \quad (6)$$

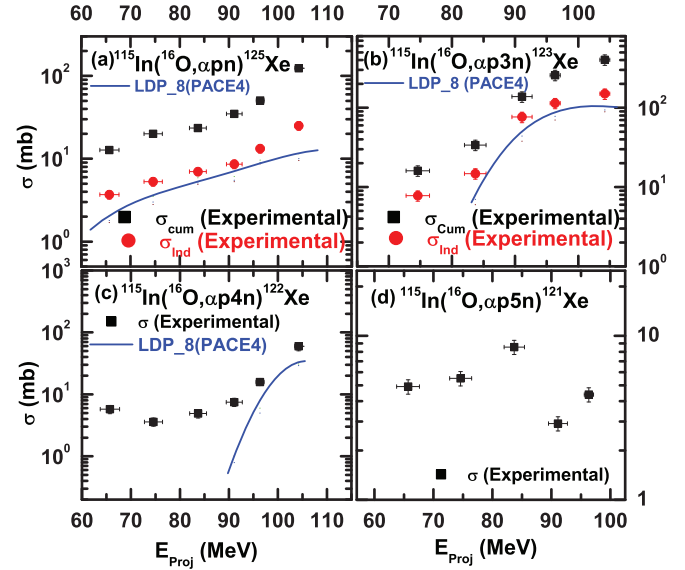


FIG. 5. (Color online) Experimentally measured EFs of all ( $\alpha pxn$ ) ( $x = 1, 3-5$ ) channels are shown and compared with the theoretical predictions of code PACE4. The cumulative yields of  $^{125}\text{Xe}$  and  $^{123}\text{Xe}$  are also exhibited.

The evaluated yields of  $^{127}\text{Cs}$  and  $^{125}\text{Cs}$  residues are listed in Table II.

Similarly, EFs for  $\alpha pxn$  channels have been plotted and shown in Figs. 5(a)–5(d). Residues  $^{125}\text{Xe}$  and  $^{123}\text{Xe}$  have contribution from their higher charge isobar precursors. Therefore, the independent yields of these residues can also be evaluated using the following equations:

$$\sigma_{\text{cum}}(^{125}\text{Xe}) = \sigma_{\text{ind}}(^{125}\text{Xe}) + 1.046\sigma_P(^{125}\text{Cs}). \quad (7)$$

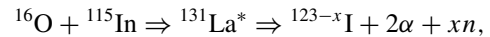
$$\sigma_{\text{cum}}(^{123}\text{Xe}) = \sigma_{\text{ind}}(^{123}\text{Xe}) + 1.051\sigma_P(^{123}\text{Cs}). \quad (8)$$

The evaluated yields of these residues along with those of  $^{122}\text{Xe}$  and  $^{121}\text{Xe}$  are also listed in Tables II and IV.

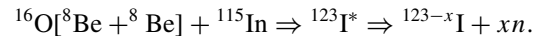
## 2. $2\alpha$ -emitting channels

Similarly, the reaction mechanism for the population of all observed  $2\alpha$ -emitting channels is also expected to be via CF and/or ICF and can be represented as

(i) CF of  $^{16}\text{O}$ , i.e.,



(ii) ICF of  $^8\text{Be}$ , i.e.,



( $2\alpha$  and/or  $^8\text{Be}$  as spectator).

The EFs of these residues are shown in Figs. 6(a)–6(c). Residue  $^{121}\text{I}$  has the contribution from its higher charge isobar precursor. Hence, its independent yield has been evaluated using the following equation:

$$\sigma_{\text{cum}}(^{121}\text{I}) = \sigma_{\text{ind}}(^{121}\text{I}) + 1.46\sigma_P(^{121}\text{Xe}). \quad (9)$$

Residue  $^{120}\text{I}$  possesses both ground and metastable state. The yields of these residues are tabulated in Table IV, along with those of  $^{119}\text{I}$ .

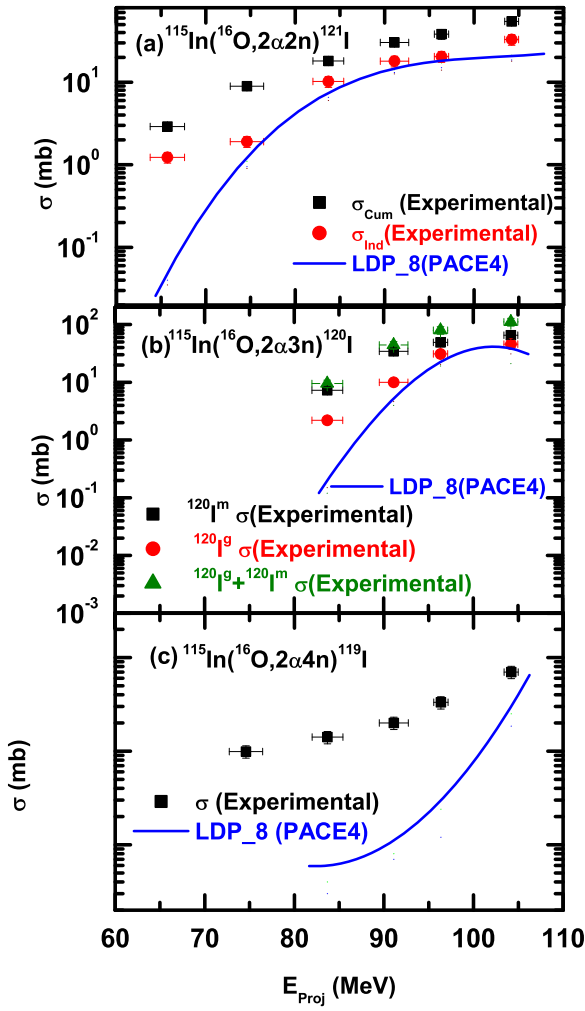


FIG. 6. (Color online) Experimentally measured EFs of  $(2\alpha xn)$  ( $x = 2-4$ ) channels are shown and compared with the theoretical predictions of code PACE4. The cumulative yield of  $^{121}\text{I}$  residue along with the ground state and metastable yields of  $^{120}\text{I}$  residue is also shown.

### 3. $3\alpha$ -emitting channels

In the same way as the  $\alpha$ - and  $2\alpha$ -emitting channels, the reaction mechanism for the population of all observed  $3\alpha$ -emitting channels can also be represented as

(i) CF of  $^{16}\text{O}$ , i.e.,



TABLE IV. Experimentally measured production reaction cross sections  $\sigma$  (mb) for  $\alpha$ -,  $2\alpha$ -, and  $3\alpha$ -emitting channels.

$E_{\text{lab}}$ (MeV)	$^{121}\text{Xe}$ (mb)	$^{121}\text{I}$ (mb)	$^{120}\text{I}^{g+m}$ (mb)	$^{119}\text{I}$ (mb)	$^{118}\text{Sb}^m$ (mb)	$^{117}\text{Sb}$ (mb)	$^{116}\text{Sb}^m$ (mb)
$65.7 \pm 1.93$	$4.9 \pm 0.53$	$1.23 \pm 0.18$			$2.18 \pm 0.32$	$3.62 \pm 0.54$	
$74.6 \pm 1.87$	$5.5 \pm 0.51$	$1.91 \pm 0.28$			$5.7 \pm 0.86$	$4.2 \pm 0.63$	
$83.2 \pm 1.72$	$8.5 \pm 0.82$	$10.2 \pm 1.53$	$9.5 \pm 1.4$	$1.41 \pm 0.21$	$12.3 \pm 1.84$	$7.3 \pm 1.09$	$1.32 \pm 0.14$
$91.1 \pm 1.6$	$2.92 \pm 0.33$	$18.0 \pm 2.7$	$44.3 \pm 6.6$	$2.0 \pm 0.33$	$10.7 \pm 1.5$	$8.5 \pm 1.28$	$3.2 \pm 0.38$
$96.35 \pm 0.8$	$4.39 \pm 0.55$	$20.5 \pm 3.07$	$80.0 \pm 12.7$	$3.32 \pm 0.49$	$15.1 \pm 2.27$	$12.5 \pm 1.88$	$4.13 \pm 0.54$
$105 \pm 0.78$		$33.0 \pm 4.95$	$111.2 \pm 16.7$	$7.0 \pm 1.05$	$20.3 \pm 3.1$	$23.5 \pm 3.4$	$6.98 \pm 1.02$

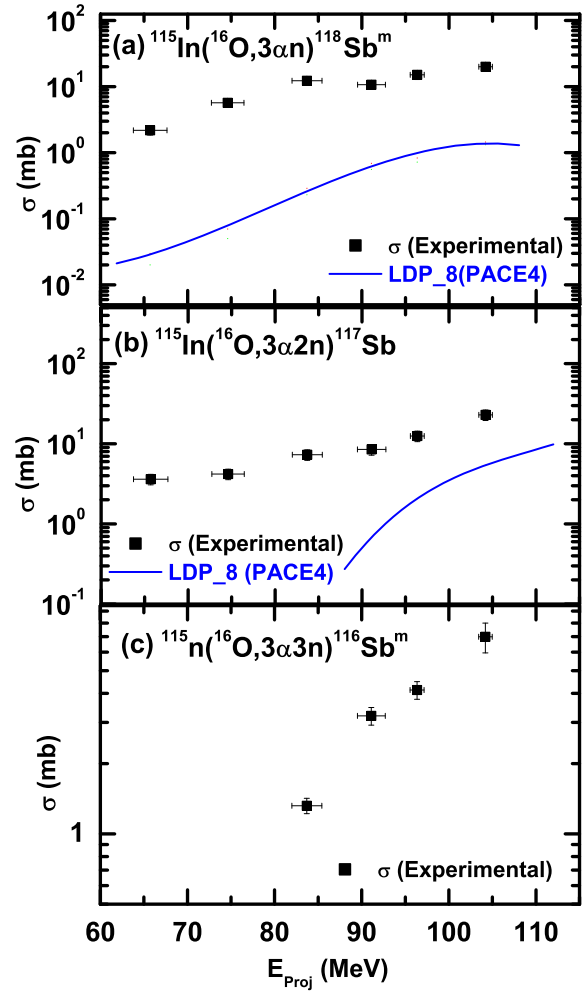


FIG. 7. (Color online) Experimentally measured EFs of all  $(3\alpha xn)$  ( $x = 1-3$ ) channels are shown and compared with the theoretical predictions of code PACE4.

(ii) ICF of  $^4\text{He}$ , i.e.,



( $3\alpha$  and/or  $^{12}\text{C}$  as spectator).

All the three residues have the ICF contribution, and their experimentally measured cross sections are tabulated in Table IV. For residue  $^{116}\text{Sb}^m$ , the theoretical predictions of code PACE4 give an almost negligible cross sections and hence are not shown. These measured excitation functions are exhibited in Figs. 7(a)–7(c).

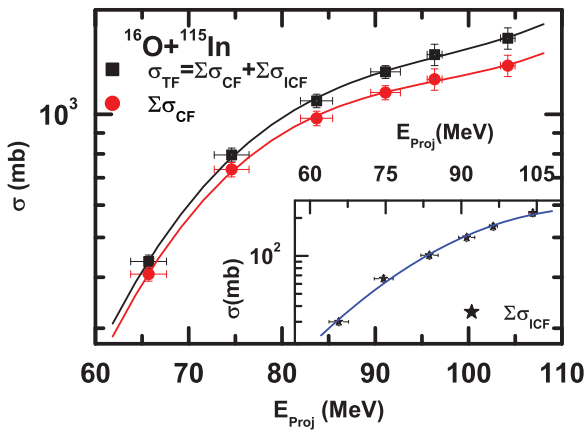


FIG. 8. (Color online) The total fusion cross section ( $\sigma_{\text{TF}}$ ) and the sum of the CF cross section ( $\Sigma\sigma_{\text{CF}}$ ) of all channels are plotted as a function of incident projectile energy. In the inset, the sum of all the ICF cross section ( $\Sigma\sigma_{\text{ICF}}$ ) at studied energies is plotted. Different solid lines through the data points are drawn to guide the eyes.

From the EFs of all the  $\alpha$ -,  $2\alpha$ -, and  $3\alpha$ -emitting channels, we can see enhancement over the theoretical predictions of PACE4. Since the statistical model code PACE4 does not take into account ICF processes, the observed enhancement in the experimentally measured EFs points toward the contribution of ICF in the production of these residues. Hence, an attempt has been made to study the ICF probability. The ICF contribution in the production of all  $\alpha$ -emitting channels has been deduced as  $\Sigma\sigma_{\text{ICF}} = \Sigma\sigma_{\text{expt.}} - \Sigma\sigma_{\text{PACE4}}$ . In order to see how does ICF contributes to the total fusion cross section ( $\sigma_{\text{TF}} = \Sigma\sigma_{\text{CF}} + \Sigma\sigma_{\text{ICF}}$ ), the sum of CF cross sections of all channels ( $\Sigma\sigma_{\text{CF}}$ ) and  $\sigma_{\text{TF}}$  as a function of incident projectile energy are plotted in Fig. 8. Different solid lines are drawn to guide the eyes. The increasing separation between  $\Sigma\sigma_{\text{CF}}$  and  $\sigma_{\text{TF}}$  indicates the energy dependence of projectile breakup. For better visualization of increasing ICF contribution with projectile energy, the value of  $\Sigma\sigma_{\text{ICF}}$  is plotted in the inset of Fig. 8. Evaluated values of  $\Sigma\sigma_{\text{CF}}$ ,  $\sigma_{\text{TF}}$ , and  $\Sigma\sigma_{\text{ICF}}$  at different energies are tabulated in Table V.

To study the dependence of ICF on different entrance channel parameters the percentage ICF fraction ( $\% F_{\text{ICF}}$ ) has been deduced for  $^{16}\text{O}+^{115}\text{In}$  system. The  $F_{\text{ICF}}$  is a measure of relative strength of ICF to the total fusion and defined as  $F_{\text{ICF}}(\%) = \frac{\Sigma\sigma_{\text{ICF}}}{\sigma_{\text{TF}}} \times 100$ . The calculated percentage ICF fraction at different incident energies has been listed in Table V.

TABLE V. Experimentally measured  $\Sigma\sigma_{\text{CF}}$ ,  $\Sigma\sigma_{\text{ICF}}$ ,  $\sigma_{\text{TF}}$ , and  $F_{\text{ICF}}(\%)$ .

$E_{\text{lab}}$ (MeV)	$\Sigma\sigma_{\text{CF}}$ (mb)	$\Sigma\sigma_{\text{ICF}}$ (mb)	$\sigma_{\text{TF}}$ (mb)	$F_{\text{ICF}}$ (%)
$65.7 \pm 1.9$	407	30.3	437.3	6.8
$74.6 \pm 1.8$	733	63.5	796.5	8.2
$83.2 \pm 1.7$	978	101.1	1079.1	9.3
$91.1 \pm 1.6$	1130	140.2	1270.2	11.0
$96.35 \pm 0.9$	1218	181.4	1399.4	12.9
$105 \pm 0.8$	1316	219.7	1535.7	14.2

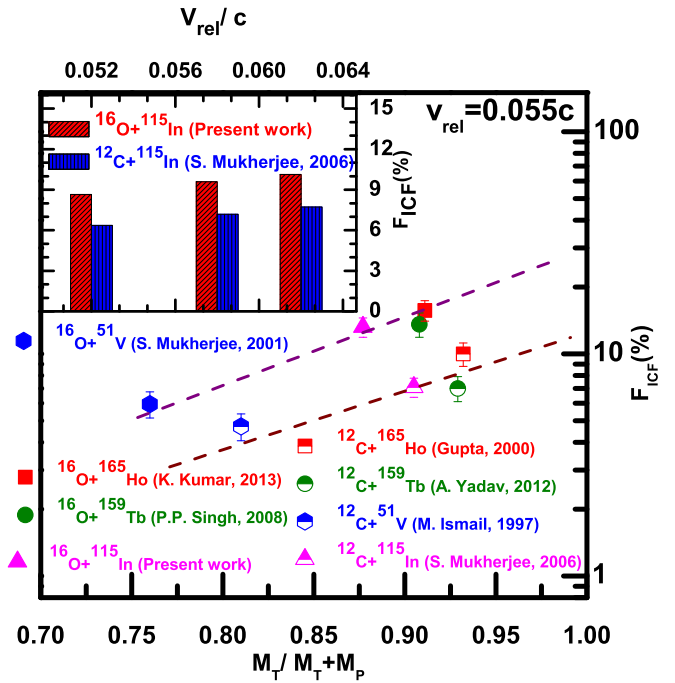


FIG. 9. (Color online) Deduced percentage ICF fraction ( $F_{\text{ICF}}$ ) for the present system as a function of mass asymmetry at  $v_{\text{rel}} = 0.055c$  is plotted along with previously available results (Ismail [28], Kumar [31], Gupta [33], Singh [34], Mukherjee [35], Singh [36], and Mukherjee [37]). In the inset, the deduced ICF fraction for the present system has been plotted at different relative velocities along with those of Mukherjee [35]. The two dashed lines are drawn to guide the eyes.

### C. Mass-asymmetry systematics and projectile structure effect

In their observations, Morgenstern *et al.* [29] found that the ICF reaction dynamics is governed by the relative velocity ( $v_{\text{relative}}$ ) of the projectile and mass asymmetry [ $\mu_a = M_T / (M_T + M_P)$ ] of interacting partners. An attempt has also been made to investigate the effect of mass-asymmetry systematics. In Fig. 9, the value of  $F_{\text{ICF}}$  of the present system  $^{16}\text{O}+^{115}\text{In}$  is plotted along with those of obtained in Refs. [28,31,33–37] at a constant relative velocity (i.e.,  $v_{\text{rel}} = 0.055c$ ). The data points suggest more ICF probability for more mass asymmetric than symmetric systems, which is in accordance with results of Morgenstern *et al.* In Fig. 9, the upper line follows  $^{16}\text{O}$ -projectile-induced reactions with  $^{51}\text{V}$ ,  $^{115}\text{In}$ ,  $^{159}\text{Tb}$ , and  $^{165}\text{Ho}$  targets and the lower line follows  $^{12}\text{C}$ -projectile-induced reactions with the same targets. This shows that  $^{12}\text{C}$ -induced reactions have less ICF fraction than  $^{16}\text{O}$ -induced reactions. Hence, it is not out of place to mention that the projectile structure effect also accounts for ICF reactions.

This projectile structure effect can be examine in terms of  $\alpha$ - $Q$  value of the projectile, as suggested in the previous reports [30–32]. These studies exhibit that for low  $\alpha$ - $Q$  value projectile ICF probability is more. Hence, to provide more strength to this aspect for  $\alpha$ -cluster projectiles in the medium mass target region, the present work has been undertaken. In order to assess this behavior of projectile structure effect, the  $F_{\text{ICF}}$  for the  $^{12}\text{C}+^{115}\text{In}$  [35] system along with that of the

present work at different relative velocities has been plotted in the inset of Fig. 9. The calculated  $\alpha$ - $Q$  values for the projectile fragmentation are  $-7.16$  MeV and  $-7.37$  MeV for  $^{16}\text{O}$  and  $^{12}\text{C}$  projectiles, respectively, making  $^{16}\text{O}$  more unstable in this regard than  $^{12}\text{C}$  in the nuclear field of the same target ( $^{115}\text{In}$ ). The obtained trend is found consistent with the previous studies [30–32]. Hence, the  $\alpha$ - $Q$  value may be responsible for this projectile structure effect, shown in Fig. 9. Moreover, it may be worth mentioning that along with mass asymmetry of interacting partners the projectile structure effect (which predominantly depends on the  $\alpha$ - $Q$  value of the projectile) also plays an important role in the ICF reaction dynamics. Furthermore, to have a more clear picture about the projectile structure effect on ICF reaction dynamics, some more refined experiments are required.

#### D. Observation of incomplete fusion contribution at $\ell < \ell_{\text{crit}}$

A few recent studies [18,36] have observed that the results of SUMRULE model calculation [15] are not consistent for the study of low-energy ICF reaction dynamics. According to this model the probability of CF is assumed to be unity for  $\ell < \ell_{\text{crit}}$  and expected to be zero  $\ell > \ell_{\text{crit}}$ . Hence, in view of the recent observation of Yadav *et al.* [18], we have measured the  $\ell_{\text{crit}}$  for the studied system  $^{16}\text{O}+^{115}\text{In}$ , using the same formula given in that reference, which is found to be  $42\hbar$ . Moreover, the theoretically calculated values of  $\ell_{\text{max}}$  for the fusion to take place at the studied energies using the statistical model code PACE4 are  $21\hbar$ ,  $31\hbar$ ,  $38\hbar$ ,  $43\hbar$ ,  $46\hbar$ , and  $50\hbar$ , respectively, as shown in Table III. The first three values of  $\ell_{\text{max}}$  are less than the estimated value of  $\ell_{\text{crit}}$  i.e.,  $42\hbar$ . However, from Table V, we can also see that even for these energies the ICF contribution is significant. This is an evidence of occurrence of ICF contribution at  $\ell < \ell_{\text{crit}}$  for the present studied system. The underestimation of the ICF cross section by the SUMRULE model may be due to the assumption in the model that a major contribution to the ICF reactions comes from the collision

trajectories with the angular momentum  $\ell$  greater than the critical angular momentum for complete fusion ( $\ell_{\text{crit}}$ ).

## IV. CONCLUSIONS

To observe the influence of entrance channel parameters on ICF reaction dynamics, an attempt has been made to measure the EFs for the production of radio nuclides,  $^{129g,129m,128-126}\text{Ba}(pxn, x=1-4)$ ,  $^{127,125}\text{Cs}(\alpha xn, x=0,2)$ ,  $^{125,123-121}\text{Xe}(\alpha pxn, x=1,3-5)$ ,  $^{121,120g,120m,119}\text{I}(2\alpha xn, x=2-4)$ , and  $^{118m,117,116m}\text{Sb}(3\alpha xn, x=1-3)$  in the energy range  $\approx 4-7$  MeV/nucleon. The experimentally measured EFs are compared with the predictions of the statistical model code PACE4, and EFs for all the CF channels are consistent with the PACE4 predictions. During the analysis, it has been found that some of the  $pxn$  and  $\alpha$ -emitting channels have contributions from their higher charge isobar precursors, which have been reduced to get the independent yield of the respective evaporation residues. In the present work the influence of different entrance channel parameters on ICF reaction dynamics has been studied. The projectile structure effect on ICF processes has been found to be understandable in terms of  $\alpha$ - $Q$  value of the projectile. Moreover, the present study also indicates the ICF contribution even at input angular momentum values  $\ell < \ell_{\text{crit}}$ . Many other entrance channel parameters may affect ICF reactions, and hence more systematic studies are required using different target-projectile combinations.

## ACKNOWLEDGMENTS

The authors thank the IUAC, New Delhi, India, for immense support during the experiment and analysis. We give our sincere thank to the Department of Physics, AMU, Aligarh, India, for providing all necessary facilities. K.K. and S.A. extend their gratitude towards the UGC for the financial support.

- 
- [1] M. Dasgupta *et al.*, *Phys. Rev. C* **66**, 041602(R) (2002).  
 [2] F. Amorini *et al.*, *Phys. Rev. C* **58**, 987 (1998).  
 [3] F. K. Amanuel, B. Zelalem, A. K. Chaubey, A. Agarwal, I. A. Rizvi, A. Maheshwari, and T. Ahmed, *Phys. Rev. C* **84**, 024614 (2011).  
 [4] P. R. S. Gomes, R. Linares, J. Lubian, C. C. Lopes, E. N. Cardozo, B. H. F. Pereira, and I. Padron, *Phys. Rev. C* **84**, 014615 (2011).  
 [5] F. K. Amanuel *et al.*, *Eur. Phys. J. A* **47**, 156 (2011).  
 [6] A. Diaz-Torres, D. J. Hinde, J. A. Tostevin, M. Dasgupta, and L. R. Gasques, *Phys. Rev. Lett.* **98**, 152701 (2007).  
 [7] P. R. S. Gomes *et al.*, *Phys. Rev. C* **73**, 064606 (2006); *Phys. Lett. B* **601**, 20 (2004).  
 [8] E. Z. Buthelezi *et al.*, *Nucl. Phys. A* **734**, 553 (2004).  
 [9] M. Dasgupta *et al.*, *Nucl. Phys. A* **787**, 144 (2007).  
 [10] D. J. Hinde, M. Dasgupta, B. R. Fulton, C. R. Morton, R. J. Wooliscroft, A. C. Berriman, and K. Hagino, *Phys. Rev. Lett.* **89**, 272701 (2002).  
 [11] D. J. Hinde, R. du Rietz, M. Dasgupta, R. G. Thomas, and L. R. Gasques, *Phys. Rev. Lett.* **101**, 092701 (2008).  
 [12] R. du Rietz *et al.*, *Phys. Rev. Lett.* **106**, 052701 (2011), and references therein.  
 [13] S. Heinz *et al.*, *Eur. Phys. J. A* **43**, 181 (2010).  
 [14] R. G. Thomas *et al.*, *Phys. Rev. C* **77**, 034610 (2008).  
 [15] J. Wilczynski *et al.*, *Nucl. Phys. A* **373**, 109 (1982).  
 [16] K. Siwek-Wilczynska, E. H. du Marchievan Voorthuysen, J. van Popta, R. H. Siemssen, and J. Wilczynski, *Phys. Rev. Lett.* **42**, 1599 (1979).  
 [17] J. R. Wu and I. Y. Lee, *Phys. Rev. Lett.* **45**, 8 (1980).  
 [18] A. Yadav *et al.*, *Phys. Rev. C* **85**, 064617 (2012).  
 [19] H. C. Britt and A. R. Quinton, *Phys. Rev.* **124**, 877 (1961).  
 [20] T. Inamura *et al.*, *Phys. Lett. B* **68**, 51 (1977).  
 [21] T. Udagawa and T. Tamura, *Phys. Rev. Lett.* **45**, 1311 (1980).  
 [22] J. P. Bondroff, *Nucl. Phys. A* **333**, 285 (1980).  
 [23] V. I. Zagrebaev, *Ann. Phys. (N.Y.)* **197**, 33 (1990).

- [24] R. Weiner *et al.*, *Nucl. Phys. A* **286**, 282 (1977).
- [25] D. J. Parker, J. J. Hogan, and J. Asher, *Phys. Rev. C* **39**, 2256 (1989).
- [26] T. Ahmad *et al.*, *Int. J. Mod. Phys. E* **20**, 645 (2011).
- [27] Avinash Agarwal *et al.*, *Int. J. Mod. Phys. E* **17**, 393 (2008).
- [28] A. Yadav *et al.*, *Phys. Rev. C* **85**, 034614 (2012).
- [29] H. Morgenstern, W. Bohne, W. Galster, K. Grabisch, and A. Kyanowski, *Phys. Rev. Lett.* **52**, 1104 (1984).
- [30] A. Yadav *et al.*, *Phys. Rev. C* **86**, 014603 (2012).
- [31] K. Kumar *et al.*, *Phys. Rev. C* **87**, 044608 (2013).
- [32] S. Ali *et al.* (unpublished).
- [33] S. Gupta, B. P. Singh, M. M. Musthafa, H. D. Bhardwaj, and R. Prasad, *Phys. Rev. C* **61**, 064613 (2000).
- [34] M. Ismail, R. P. Sharma, and M. H. Rashid, *Parmana* **49**, 623 (1997).
- [35] S. Mukherjee *et al.*, *Int. J. Mod. Phys. E* **15**, 237 (2006).
- [36] P. P. Singh, B. P. Singh, M. K. Sharma, Unnati, D. P. Singh, R. Prasad, R. Kumar, and K. S. Golda, *Phys. Rev. C* **77**, 014607 (2008).
- [37] S. Mukherjee *et al.*, *Eur. Phys. J. A* **12**, 199 (2001).
- [38] Stopping and Range of Ions in Matter (SRIM) code: <http://www.srim.org/SRIM/SRIMLEGL.htm>.
- [39] Freedom data acquisition and analysis system designed to support the accelerator-based experiments at the Interuniversity Accelerator Center (IUAC), New Delhi, India.
- [40] E. Browne and R. B. Firestone, *Table of Radioactive Isotopes* (Wiley, New York, 1986).
- [41] P. R. S. Gomes *et al.*, *Nucl. Phys. A* **834**, 151C (2010).
- [42] J. M. B. Shorto *et al.*, *Phys. Lett. B* **678**, 77 (2009).
- [43] A. Gavron, *Phys. Rev. C* **21**, 230 (1980).
- [44] S. F. Mughabghab, M. Divadeenam, and N. E. Holden, *Neutron Cross-Sections* (Academic Press, New York, 1981), Vol. 1, Part A, p. 89.
- [45] M. Cavinato *et al.*, *Phys. Rev. C* **52**, 2577 (1995).
- [46] H. Feshbach and V. F. Weisskopf, *Phys. Rev.* **76**, 1550 (1949); H. Feshbach *et al.*, *ibid.* **96**, 448 (1954).
- [47] R. Bass, *Nucl. Phys. A* **231**, 45 (1974).
- [48] F. D. Becchetti and G. W. Greenlees, *Phys. Rev.* **182**, 1190 (1969).
- [49] G. R. Satchler, *Nucl. Phys.* **70**, 177 (1965).
- [50] P. M. Endt, *At. Data Nucl. Data Tables* **26**, 47 (1981).
- [51] S. K. Kataria, V. S. Ramamurthy, and S. S. Kapoor, *Phys. Rev. C* **18**, 549 (1978).
- [52] D. Fabris *et al.*, *Phys. Rev. C* **50**, R1261 (1994).
- [53] H. H. Gutbrod, W. G. Winn, and M. Blann, *Phys. Rev. Lett.* **30**, 25 (1973).